Electron-Tunneling Paths in Various Electrostatic Complexes between Cytochrome *c* and Plastocyanin. Anisotropy of the Copper-Ligand Interactions and Dependence of the Iron-Copper Electronic Coupling on the Metalloprotein Orientation

G. Matthias Ullmann and Nenad M. Kostić*

Contribution from the Department of Chemistry, Iowa State University, Ames, Iowa 50011

Received June 20, 1994[⊗]

Abstract: The *Pathways* method of Beratan and Onuchic is applied to analysis and comparison of electron-tunneling paths between the iron(II) and copper(II) sites in six configurations of the complex between ferrocytochrome *c* and cupriplastocyanin. Standard parametrization is used, and electronic coupling in aromatic rings is treated as both attenuated and unattenuated; the results did not signifiantly depend on this choice. In one methodological improvement, crystallographically detected water molecules are included inside the proteins, and the vicinity of the protein-protein interface is hydrated in a molecular simulation. In another improvement, anisotropy of metal-ligand electronic coupling in the blue copper site is explicitly recognized. Standard calculations, in which the copper(II)-ligand coupling is treated as isotropic, showed the so-called northern equatorial configuration to have the greatest iron(II)-copper(II) coupling, i.e., the best tunneling paths. Other configurations provide neither few excellent paths nor many good ones. Scaled calculations, in which the anisotropy of the copper(II)-ligand coupling is treated in three different ways, favor the paths ending with Cys 84 and disfavor or abolish those ending with the other three ligands. These scaled calculations consistently showed the northern equatorial and the so-called "maximum-overlap, rotated" configurations to have greater coupling than the other electrostatically-stabilized configurations of the diprotein complex. The so-called maximum-overlap configuration, which has optimal electrostatic docking, lags behind the other two configurations in electronic coupling. Calculations of electronic coupling of the iron(II) and copper(II) sites to the surfaces of the respective proteins and matching of the surface patches in the two proteins were consistent with the analysis of iron(II)-copper(II) couplings. There are steric obstacles to contacts between the "conductive" surface patches in the maximum-overlap configuration but not in the northern equatorial configuration. This theoretical study corroborates experimental findings in this laboratory that the diprotein complex with optimal electrostatic *interactions* is not optimal for the intracomplex electron-transfer *reactions*. In studies of metalloprotein complexes by the *Pathways* method, internal and external hydration, anisotropy of metal-ligand coupling, and steric effects should all be considered.

Introduction

Little is known about the effects of protein-protein orientation and docking mode on electron-transfer reactions between metalloproteins.[1-12] These effects can be thoroughly studied with cytochrome *c* and plastocyanin because three-dimensional structures of both of these proteins, in both oxidized and reduced forms and in both solid state (X-ray crystallography) and solution (NMR spectroscopy), are known in detail. The blue copper protein plastocyanin is notable because it has on its surface two distinct areas through which it can exchange electrons with redox partners.[13-15] The broad and negatively charged acidic patch is remote from the copper site, whereas the smaller and electroneutral hydrophobic patch is proximate to this site. The heme protein cytochrome *c* has on its surface only one area, the positively charged basic patch surrounding the slightly exposed heme edge, through which it can exchange electrons with redox partners.[16] There is much evidence that in the electrostatic complex cytochrome *c*/plastocyanin (cyt/pc) the basic patch in cytochrome *c* abuts the acidic patch in plastocyanin,[17-19] although this description in terms of the two broad patches does not precisely define the config-

[⊗] Abstract published in *Advance ACS Abstracts,* April 15, 1995.

(1) Hoffman, B. M.; Natan, M. J.; Nocek, J. M.; Wallin, S. A. *Struct. Bonding* **1991**, *75*, 86.
(2) McLendon, G. *Struct. Bonding* **1991**, *75*, 160.
(3) McLendon, G. *Metal Ions Biol. Syst.* **1991**, *27*, 183.
(4) McLendon, G.; Hake, R. *Chem. Rev.* **1992**, *92*, 481.
(5) Therien, M. J.; Chang, J.; Raphael, A. L.; Bowler, B. E.; Gray, H. B. *Struct. Bonding* **1991**, *75*, 110.
(6) Winkler, J. R.; Gray, H. B. *Chem. Rev.* **1992**, *92*, 369.
(7) Mauk, A. G. *Struct. Bonding* **1991**, *75*, 131.
(8) Kostić, N. M. *Metal Ions Biol. Syst.* **1991**, *27*, 129.
(9) Willie, A.; McLean, M.; Liu, R.-Q.; Hilgen-Willis, S.; Saunders, A. J.; Pielak, G. J.; Sligar, S. G.; Durham, B.; Millett, F. *Biochemistry* **1993**, *32*, 7519.
(10) Kuznetsov, A. M.; Ulstrup, J. *J. Electroanal. Chem.* **1989**, *275*, 289.
(11) Andrew, S. M.; Thomasson, K. A.; Northrup, S. H. *J. Am. Chem. Soc.* **1993**, *115*, 5516.
(12) Northrup, S. H.; Thomasson, K. A.; Miller, C. M.; Barker, P. D.; Eltis, L. D.; Guillemette, J. G.; Inglis, S. C.; Mauk, A. G. *Biochemistry* **1993**, *32*, 6613.
(13) (a) Sykes, A. G. *Struct. Bonding* **1991**, *75*, 177. (b) Sykes, A. G. *Adv. Inorg. Chem.* **1991**, *36*, 377.
(14) Christensen, H. E. M.; Conrad, L. S.; Ulstrup, J.; Mikkelsen, K. V. *Metal Ions Biol. Syst.* **1991**, *27*, 57.
(15) Redinbo, M. R.; Yeates, T. O.; Merchant, S. *J. Bioenerg. Biomembr.* **1994**, *26*, 49.
(16) Moore, G. R.; Pettigrew, G. W. *Cytochromes c: Evolutionary, Structural and Physicochemical Aspects*; Springer-Verlag: Berlin, 1990.
(17) Bagby, S.; Driscoll, P. C.; Goodall, K. G.; Redfield, C.; Hill, H. A. O. *Eur. J. Biochem.* **1990**, *188*, 413.
(18) Roberts, V. A.; Freeman, H. C.; Getzoff, E. D.; Olson, A. J.; Tainer, J. A. *J. Biol. Chem.* **1991**, *266*, 13431.
(19) Zhou, J. S.; Brothers, H. M., II; Neddersen, J. P.; Cotton, T. M.; Peerey, L. M.; Kostić, N. M. *Bioconjugate Chem.* **1992**, *3*, 382.

0002-7863/95/1517-4766$09.00/0

uration of the diprotein complex. There is, however, considerable evidence that the docking configuration is not the same as the reactive one, i.e., that the diprotein complex must rearrange for the intracomplex electron-transfer reactions in eqs 1−3.[20−28]

$$\text{cyt(II)/pc(II)} \rightarrow \text{cyt(III)/pc(I)} \quad (1)$$

$$^3\text{Zncyt/pc(II)} \rightarrow \text{Zncyt}^+\text{/pc(I)} \quad (2)$$

$$^3\text{Sncyt/pc(II)} \rightarrow \text{Sncyt}^+\text{/pc(I)} \quad (3)$$

(The Roman numerals are the oxidation states of iron and copper.) The rate of this rearrangement, 2×10^5 s^{-1}, was determined by analyzing effects of solvent viscosity on the photoinduced electron-transfer reactions in eqs 2 and 3.[23,26] This same rate probably applies also to the thermal reaction in eq 1 because replacement of iron(II) by zinc(II) and tin(IV) in cytochrome *c* does not noticeably alter the electrostatic properties and topography of the protein surface.[29−31] The two photoinduced reactions are gated because the protein rearrangement is much slower than the electron-transfer step. The thermal reaction, however, is not gated because the rearrangement is much faster than the electron-transfer step.[23,26]

The nature of the rearrangement process was elucidated in the study of the photoinduced reaction in eq 4, which is

$$^3\text{Zncyt/b}_5\text{(III)} \rightarrow \text{Zncyt}^+\text{/b}_5\text{(II)} \quad (4)$$

comparable with that in eq 2. Electrostatic complexes which zinc(II) cytochrome *c* forms with plastocyanin and with cytochrome b_5 turned out to have virtually identical rearrangement rates even though plastocyanin has two distinct reactive patches on its surface, whereas cytochrome b_5 has only one—the negatively charged (acidic) patch around the exposed heme edge.[32] Migration of cytochrome *c* on the plastocyanin surface away from the acidic patch and fluctuation within the general docking configuration while the exposed heme edge remains within or near the extensive acidic patch are not conceptually different processes. The two dynamical processes—migration and fluctuation—differ in degree more than in kind.[32]

Here we investigate the cause of rearrangement. In particular, we test the hypothesis that the electrostatic complex cyt/pc rearranges in order to optimize electronic coupling between the iron and copper sites. We apply the *Pathways* method of Beratan and Onuchic,[33−39] which allows identification of paths (often called pathways) for electron tunneling through the inhomogeneous barrier that the protein represents. Search for the dominant set of interactions via covalent bonds, hydrogen bonds, and van der Waals contacts between two points in the protein yields estimates of relative magnitudes of electronic coupling along different paths in the static system. This method has successfully been applied to the study of several metalloproteins with and without attached redox-active metal complexes,[40−48] and it is being improved from both the theoretical and computational points of view. An alternative method is also being used.[49]

The *Pathways* method is only beginning to be applied to protein complexes. Although the two previous studies of this kind were small, they are valuable because they dealt with interesting and important complexes. One was the binary complex of cytochrome *c* and cytochrome *c* peroxidase,[42] and the other was the ternary complex of methylamine dehydrogenase, amicyanin, and cytochrome c_{551i}.[50] We think that the *Pathways* method is especially suitable for analysis of protein complexes because in these systems both the electron donor and the electron acceptor are embedded in the protein matter, which lends itself well to analysis of electronic coupling. Here we analyze the cyt/pc system in detail by comparing different static configurations of this system in order to understand its dynamics. We propose two improvements in the *Pathways* method and the computational procedure.

Theory and Computation

Calculations of Relative Coupling. Both the theoretical basis and the algorithm for the *Pathways* method are described in detail elsewhere.[33−48] We kept in mind its assumptions and approximations, but also its utility and soundness, found in previous applications. Here we briefly explain only those features that are most pertinent to our study.

Because the electron-transfer reaction in eq 1 is activated, nonadiabatic, and not gated, its rate constant (k) is proportional to the square of the electronic coupling (T_{DA}) between the donor (D) and acceptor (A) and to a nuclear (or Franck−Condon) factor describing the motion along the nuclear coordinate; see eq 5.[51] The symbol λ stands for reorganizational energy. A

$$k = \frac{2\pi}{\hbar}|T_{DA}|^2 \frac{1}{(4\pi\lambda RT)^{1/2}} \exp\left[-\frac{(\Delta G^\circ + \lambda)^2}{4\lambda RT}\right] \quad (5)$$

tunneling path is defined as a combination of interacting covalent

(20) Peerey, L. M.; Kostić, N. M. *Biochemistry* **1989**, *28*, 1861.
(21) Peerey, L. M.; Brothers, H. M., II; Hazzard, J. T.; Tollin, G.; Kostić, N. M. *Biochemistry* **1991**, *30*, 9297.
(22) Zhou, J. S.; Kostić, N. M. *J. Am. Chem. Soc.* **1991**, *113*, 7040.
(23) Zhou, J. S.; Kostić, N. M. *J. Am. Chem. Soc.* **1992**, *114*, 3562.
(24) Zhou, J. S.; Kostić, N. M. *Spectrum* **1992**, *5* (2), 1.
(25) Zhou, J. S.; Kostić, N. M. *Biochemistry* **1993**, *32*, 4539.
(26) Zhou, J. S.; Kostić, N. M. *J. Am. Chem. Soc.* **1993**, *115*, 10796.
(27) Modi, S.; He, S.; Gray, J. C.; Bendall, D. S. *Biochim. Biophys. Acta* **1992**, *1101*, 64.
(28) Modi, S.; Nordling, M.; Lundberg, L. G.; Hansson, Ö.; Bendall, D. S. *Biochim. Biophys. Acta* **1992**, *1102*, 85.
(29) Vanderkooi, J. M.; Erecińska, M. *Eur. J. Biochem.* **1975**, *60*, 199.
(30) Vanderkooi, J. M.; Adar, F.; Erecińska, M. *Eur. J. Biochem.* **1976**, *64*, 381.
(31) Moore, G.; Williams, R. J. P.; Chien, J. C. W.; Dickinson, L. C. *J. Inorg. Biochem.* **1980**, *13*, 1.
(32) Qin, L.; Kostić, N. M. *Biochemistry* **1994**, *33*, 12592.
(33) Beratan, D. N.; Onuchic, J. N.; Hopfield, J. J. *J. Chem. Phys.* **1987**, *86*, 4488.
(34) Beratan, D. N.; Onuchic, J. N. *Photosynth. Res.* **1989**, *22*, 173.
(35) Onuchic, J. N.; Beratan, D. N. *J. Chem. Phys.* **1990**, *92*, 722.
(36) Beratan, D. N.; Betts, J. N.; Onuchic, J. N. *Science* **1991**, *252*, 1285.
(37) Beratan, D. N.; Betts, J. N.; Onuchic, J. N. *J. Phys. Chem.* **1992**, *96*, 2852.
(38) Betts, J. N.; Beratan, D. N.; Onuchic, J. N. *J. Am. Chem. Soc.* **1992**, *114*, 4043.
(39) Regan, J. J.; Risser, S. M.; Beratan, D. N.; Onuchic, J. N. *J. Phys. Chem.* **1993**, *97*, 13083.
(40) Beratan, D. N.; Onuchic, J. N.; Betts, J. N.; Bowler, B.; Gray, H. B. *J. Am. Chem. Soc.* **1990**, *112*, 7915.
(41) Beratan, D. N.; Onuchic, J. N.; Gray, H. B. *Metal Ions Biol. Syst.* **1991**, *27*, 97.
(42) Onuchic, J. N.; Beratan, D. N.; Winkler, J. R.; Gray, H. B. *Science* **1992**, *258*, 1740.
(43) Onuchic, J. N.; Beratan, D. N.; Winkler, J. R.; Gray, H. B. *Annu. Rev. Biophys. Biomol. Struct.* **1992**, *21*, 349.
(44) Beratan, D. N.; Onuchic, J. N. *Advances in Chemistry Series 228*; Bolton, J. R., Mataga, N., McLendon, G., Eds.; American Chemical Society: Washington, DC, 1991; p 72.
(45) Wuttke, D. S.; Bjerrum, M. J.; Winkler, J. R.; Gray, H. B. *Science* **1992**, *256*, 1007.
(46) Cowan, J. A.; Upmacis, R. K.; Beratan, D. N.; Onuchic, J. N.; Gray, H. B. *Ann. N.Y. Acad. Sci.* **1988**, *550*, 68.
(47) Jacobs, B. A.; Mauk, M. R.; Funk, W. D.; MacGillivray, R. T. A.; Mauk, A. G.; Gray, H. B. *J. Am. Chem. Soc.* **1991**, *113*, 4390.
(48) Casimiro, D. R.; Wong, L.-L.; Colón, J. L.; Zewert, T. E.; Richards, J. H.; Chang, I.-J.; Winkler, J. R.; Gray, H. B. *J. Am. Chem. Soc.* **1993**, *115*, 1485.
(49) (a) Moser, C. C.; Keske, J. M.; Warncke, K.; Farid, R. S.; Dutton, P. L. *Nature* **1992**, *355*, 6363. (b) Farid, R. S.; Moser, C. C.; Dutton, P. L. *Curr. Opin. Struct. Biol.* **1993**, *3*, 225.
(50) Chen, L.; Durley, R. C. E.; Mathews, F. S.; Davidson, V. L. *Science* **1994**, *264*, 86.
(51) Marcus, R. A.; Sutin, N. *Biochim. Biophys. Acta* **1985**, *811*, 265.

bonds, hydrogen bonds, and van der Waals contacts (so-called interactions through space) that link the donor and the acceptor. The respective decay parameters for attenuation of electronic coupling across these bonds and contacts are the unitless quantities ϵ_C, ϵ_H, and ϵ_S, defined in eq 6 (general formula) and eqs 7–9 (specific formulas, with the parameter values). In these

$$\epsilon = \alpha \exp[-\beta(R - R_{eq})] \quad (6)$$

$$\epsilon_C = 0.6 \quad (7)$$

$$\epsilon_H = 0.36 \exp[-1.7(R - 2.8)] \quad (8)$$

$$\epsilon_S = 0.6 \exp[-1.7(R - 1.4)] \quad (9)$$

formulas, α is a prefactor, β describes the dependence of the interaction on distance, R is the distance between the centers of the interacting orbitals (in Å), and the equilibrium distances, R_{eq}, are 1.4 and 2.8 Å for covalent and hydrogen bonds, respectively. The tunneling matrix element for a single path is defined in eq 10. The total tunneling matrix element, T_{DA},

$$t_{DA} = (\text{prefactor}) \prod_i \epsilon_C(i) \prod_j \epsilon_H(j) \prod_k \epsilon_S(k) \quad (10)$$

$$= (\text{prefactor})(\text{relative coupling})$$

introduced in eq 1, includes the elements t_{DA} for the many possible paths connecting the donor and the acceptor. Because the difficult problem of the relation between t_{DA} and T_{DA} has yet to be solved, we qualitatively relate the rate of electron transfer to the efficiency of the best path according to eq 11.

$$k_{et} \propto (\text{relative coupling})^2 \quad (11)$$

The prefactor in eq 10 depends on the interactions between the electron donor and the first orbital in the path and between the electron acceptor and the last orbital in the path. The standard search for paths amounts to maximization of the triple product in eq 10, which we call relative coupling. In some searches, we followed this standard procedure, which neglects differences among the ligands bonded to the given metal atom. In other searches, we multiplied the relative couplings by different prefactors, as will be explained below.

The calculations were done with a Silicon Graphics computer SGI IRIS 4D/35 and the IRIX (UNIX) operating system 4.0.5 System V. The paths were analyzed by the program Greenpath v0.90, the version of August 1993. The proteins and the output of Greenpath were visualized by the program QUANTA 3.3, developed by Molecular Simulation, Inc., and the program INSIGHT II, developed by Biosym Technologies, Inc. The van der Waals surfaces of the separate protein molecules were calculated by the Quanta program.

Parameters. The standard values of parameters, specified in eqs 7–9, were used. Coupling within aromatic systems (heme, histidine, phenylalanine, tyrosine, and tryptophane) was defined in two ways. In one, bonds in aromatic rings were treated as the usual covalent bonds ($\epsilon = 0.6$). In the other, the enhanced coupling in aromatic rings was recognized by neglecting the attenuation ($\epsilon = 1$).

All the numerous paths with relative couplings down to 30% of that found for the best path were identified. In order to identify the even more numerous paths with relative couplings down to a much smaller fraction of that found for the best path without exceeding the computer memory, parts of the best path were "blocked" by setting to zero the ϵ_C parameters for certain bonds along the best path. This blocking removed from the tunneling paths entire residues or only their side chains (in which case the main chains could still be involved). These expanded searches with blocking were done in the most thorough investigations—those involving unattenuated coupling within aromatic systems, crystalline water in the proteins, and solvent water near the protein interface.

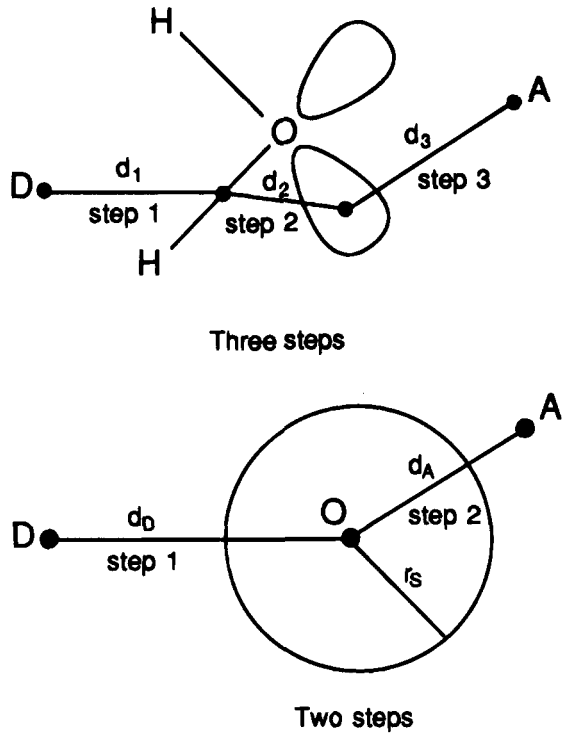

Figure 1. Coupling of donor (D) and acceptor (A) via a water molecule in three or two steps. In the former case, the hydrogen atoms and the lone pairs are explicitly recognized. In the latter case, which is more realistic, the water molecule is treated as a sphere, with the orbitals centered on the oxygen atom.

Coupling Maps. All relative couplings (defined in eq 10) between the metal atom and all the orbitals in the protein were calculated for the following proteins: cuproplastocyanin and cupriplastocyanin from polar, cuproplastocyanin from French bean, ferrocytochrome *c* and ferricytochrome *c* from tuna, and ferricytochrome *c* from horse. The structure of the French-bean plastocyanin in solution, determined by NMR spectroscopy, did not include water molecules. All the other structures were determined by X-ray crystallography and included water. Comparative calculations showed that crystallographic disorder found for several residues in the cuproplastocyanin crystals had no significant effect on relative coupling of these residues to the copper atom. Amino acid residues are classified by the magnitude of $\log_{10}(\text{relative coupling})^2$ as follows: strongly coupled, greater than −3.5; medium coupled, from −3.6 to −5.5; and weakly coupled, less than −5.5.

Treatment of Hydration. Water at the protein surface may be important for electron transfer, as was recently shown in studies of the blue copper protein azurin.[52,53] In our study two kinds of hydration are considered.

Electron tunneling from a donor D, via a water molecule, to an acceptor A can be represented as a three-step process, as in Figure 1 and eq 12. More realistically, water molecules in

$$\epsilon_{H_2O} = \alpha_1\alpha_2\alpha_3 \exp[-\beta_1(d_1 - R_{eq_1}) - \beta_3(d_3 - R_{eq_3})] \quad (12)$$

(52) Nar, H.; Messerschmidt, A.; Huber, R.; van de Kamp, M.; Canters, G. W. *J. Mol. Biol.* **1991**, *218*, 427.
(53) Mikkelsen, K. V.; Skov, L. K.; Nar, H.; Farver, O. *Proc. Natl. Acad. Sci. U.S.A.* **1993**, *90*, 5443.
(54) Pelletier, H.; Kraut, J. *Science* **1992**, *258*, 1748.

ferrocytochrome *c* and cupriplastocyanin are represented as they are found in X-ray crystallographic maps of electron density—as spheres with a radius $r_S = 1.46$ Å. Because the hydrogen atoms and the lone electron pairs cannot be resolved, the water orbitals are centered on the oxygen atom. The same electron tunneling now becomes a two-step process, as in Figure 1 and eqs 13 and 14. With standard parameters in the eqs 13 and 14 and

$$\epsilon_{H_2O}^{\text{step 1}} = \alpha_1\sqrt{\alpha_2}\exp[-\beta_1(R_1 - R_{eq_1})] \quad (13)$$

$$\epsilon_{H_2O}^{\text{step 2}} = \alpha_3\sqrt{\alpha_2}\exp[-\beta_3(R_3 - R_{eq_3})] \quad (14)$$

$$R_1 = d_D - \frac{r_S}{2} \quad (15)$$

$$R_3 = d_A - \frac{r_S}{2} \quad (16)$$

with the definition in eq 17, we finally obtain eq 18, for tunneling through a water molecule. In control calculations,

$$R_{eq_{H_2O}} = \frac{r_S}{2} + 1.4\text{ Å} = 2.13\text{ Å} \quad (17)$$

$$\epsilon_{H_2O} = 0.46\exp[-1.7(R - 2.13)] \quad (18)$$

we explicitly considered the hydrogen atoms and lone pairs and we rotated this actual water molecule. Donor—acceptor coupling varied only slightly as the orientation of the interposed water molecule changed. This finding justifies the approximations made above. Indeed, X-ray crystallography shows that water molecules inside proteins usually have high temperature factors, an indication of rapid motion.

The water molecules in the proteins were copied onto the cyt/pc complex from the crystal structures of ferrocytochrome *c*[55] and of cupriplastocyanin,[56] which have the resolutions of 1.5 and 1.6 Å, respectively. External solvation within a box sized 30 × 30 × 30 Å^3 and centered at the midpoint of the protein—protein interface was simulated by the program CHARMm, developed by Molecular Simulation, Inc. If the van der Waals surface of a water molecule overlapped with this surface of either protein, such a water molecule would be deleted. The orientations of the remaining water molecules were relaxed in structural optimizations during which the proteins coordinates were kept fixed.

Anisotropic Coupling within the Blue Copper Site. In the standard *Pathways* method, as embodied in the Greenpath program, the prefactor in eq 10 is neglected. An important consequence of this approximation in the treatment of metalloproteins is that all metal—ligand interactions are made to contribute equally to electronic coupling of the metal atom, via the ligands, to other sites. Under this approximation, it does not matter through which ligand an electron enters or leaves the metal complex. The controversial question whether proteins are isotropic barriers for electron tunneling through space[49] or anisotropic barriers for electron tunneling via discrete paths[33-48] will be easier to answer if the well-known anisotropy of metal—ligand electronic interaction is recognized in the analysis of tunneling.

Electronic structure and bonding in the active sites of blue copper proteins,[13b,57,58] and of plastocyanin in particular,[59-63] have been much studied. The redox orbital of the copper(II) complex, its half-occupied HOMO, is dominated by a π interaction between the copper(II) atom and the thiolate anion in Cys 84. Detailed quantum chemical calculations[59,60] and X-ray absorption spectroscopy[61,62] showed that this redox orbital is (de)localized approximately as follows: 42% on the $d_{x^2-y^2}$ orbital of copper(II), 46% on the sulfur atom of the thiolate anion in Cys 84, 2.3% shared equally (1.2% each) by the donor nitrogen atoms of the imidazole rings in His 37 and His 87, and practically nil on the sulfur atom of the thioether group in Met 92. Solomon and co-workers astutely realized the importance of this anisotropic covalency for the electron-transfer reactivity of plastocyanin. Newton showed that the coupling t_{DA} via a particular ligand is proportional to the square of the expansion coefficient (γ) for this ligand orbital in the molecular orbital involved in electron transfer.[64] On reasonable assumption that the aforementioned percentages are proportional to the squares of the expansion coefficients, the relative values of the coefficients of the HOMO are 0.65 for the Cu $d_{x^2-y^2}$, 0.68 for Cys 84, 0.11 for His 37, 0.11 for His 87, and 0 for Met 92.

If the anisotropy of coupling between the iron(II) atom (the electron donor) and its ligands and between the copper(II) atom (the electron acceptor) and its ligands is recognized, eq 19 should

$$t_{DA} \propto \gamma_{DL}{}^2\gamma_{AL}{}^2(\text{relative coupling}) \quad (19)$$

be used, with the assumption that the expansion coefficients γ in the redox orbital are independent of the relative coupling. Because all the paths involve the porphyrin ring, i.e., the equatorial nitrogen ligands, the quantity $\gamma_{DL}{}^2$ for cytochrome *c* is the same for all paths and was omitted from eq 20. In one

$$t_{DA} \propto \gamma_{AL}{}^2(\text{relative coupling}) \quad (20)$$

analysis, all the relative couplings found by the program were scaled according to eq 20, depending on the ligand to copper(II) that is involved. In another analysis, all the relative couplings were scaled by the expansion coefficient and not its square, as in eq 21. In yet another analysis, the high covalency

$$t_{DA} \propto \gamma_{AL}(\text{relative coupling}) \quad (21)$$

of the copper(II) bond to Cys 84 was recognized by setting $\epsilon = 1$ for this interaction. All of these calculations were done with full inclusion of internal and external water into the cyt/pc complex.

Six Configurations of the Cyt/Pc Complex. Roberts et al. developed an extremely efficient computer method for the identification of electrostatically favorable orientations (configurations) of two proteins of known structures and tested this method on tuna ferrocytochrome *c* and poplar cupriplastocyanin.[18] They calculated the electrostatic fields of both proteins and systematically analyzed 3.3 × 10^6 protein—protein orientations, seeking those with the best match of the fields and the greatest electrostatic attraction. The 1411 orientations found within 1 kcal·mol^{-1} of the most stable one were grouped in five families, which are shown in Figure 2. In different configurations the exposed heme edge in cytochrome *c* points

(55) Takano, T.; Dickerson, R. E. *J. Mol. Biol.* **1981**, *153*, 79.
(56) Guss, J. M.; Freeman, H. C. *J. Mol. Biol.* **1983**, *169*, 521.
(57) Solomon, E. I.; Baldwin, M. J.; Lowery, M. D. *Chem. Rev.* **1992**, *92*, 521.
(58) Solomon, E. I.; Lowery, M. D. *Science* **1993**, *259*, 1575.
(59) Penfield, K. W.; Gewirth, A. A.; Solomon, E. I. *J. Am. Chem. Soc.* **1985**, *107*, 4519.
(60) Gewirth, A. A.; Solomon, E. I. *J. Am. Chem. Soc.* **1988**, *110*, 3811.
(61) Shadle, S. E.; Penner-Hahn, J. E.; Schugar, H. J.; Hedman, B.; Hodgson, K. O.; Solomon, E. I. *J. Am. Chem. Soc.* **1993**, *115*, 767.
(62) George, S. J.; Lowery, M. D.; Solomon, E. I.; Cramer, S. P. *J. Am. Chem. Soc.* **1993**, *115*, 2968.
(63) Lowery, M. D.; Guckert, J. A.; Gebhard, M. S.; Solomon, E. I. *J. Am. Chem. Soc.* **1993**, *115*, 3012.
(64) Newton, M. D. *Chem. Rev.* **1991**, *91*, 767.

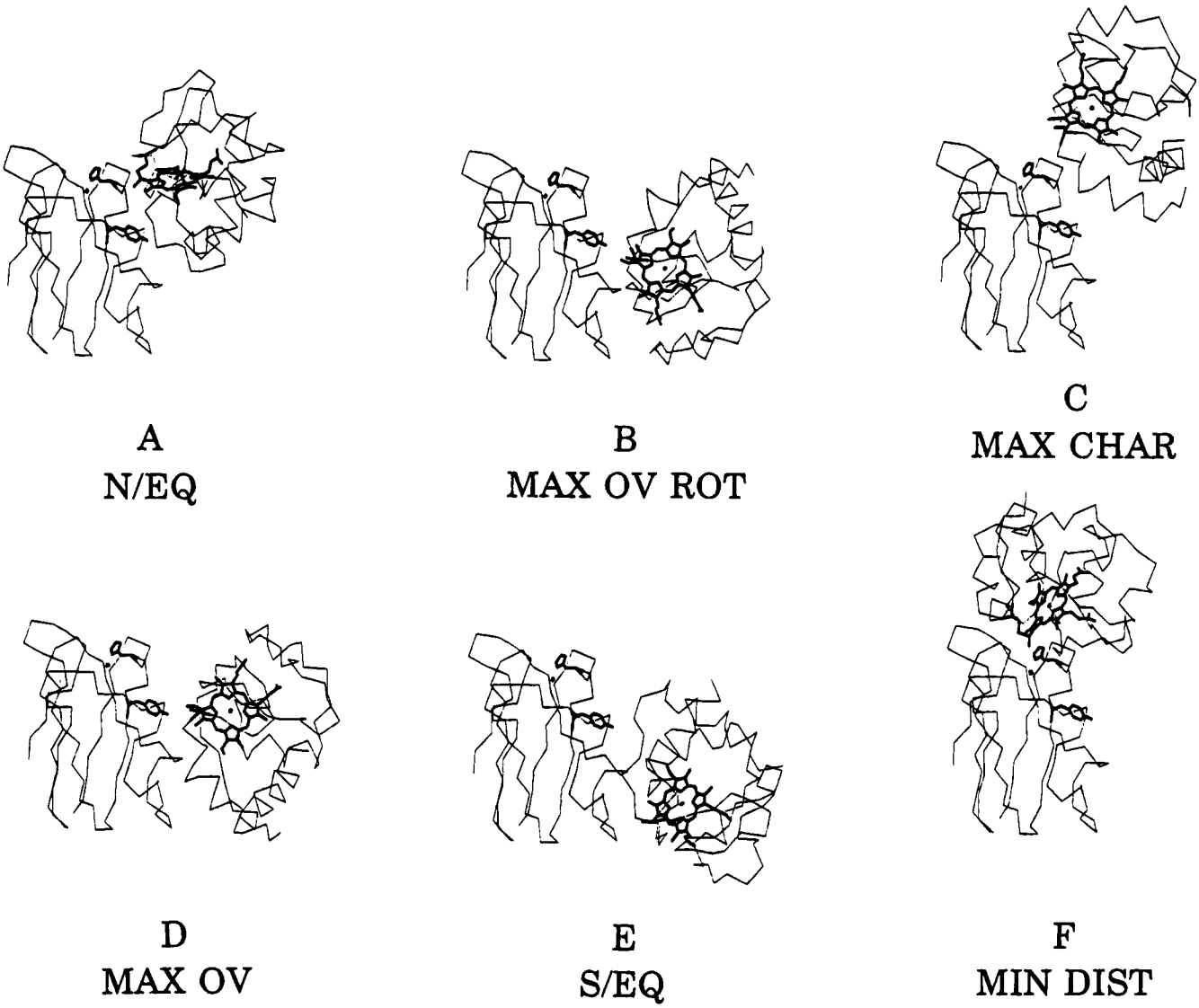

Figure 2. Six configurations of the cyt(II)/pc(II) complex found by an analysis of electrostatic interactions between the protein molecules.[18] Poplar cupriplastocyanin is on the left, in the fixed position, with highlighted Tyr 83 (in the acidic patch) and His 87 (in the hydrophobic patch). Tuna ferrocytochrome *c* is on the right, in different positions, with highlighted heme and the exposed residue Cys 17. The copper(II) and iron(II) atoms are marked with dots. (A) Northern equatorial configuration (N/EQ): the heme edge sits between the hydrophobic and acidic patches, and Cys 17 is near the former patch. (B) Maximum-overlap configuration, rotated by 180° (MAX OV ROT): the heme edge and Cys 17 point to the acidic patch, and the heme edge is near Tyr 83. (C) Maximum-charge configuration (MAX CHAR): the area around Lys 27 in ferrocytochrome *c* abuts the upper part of the acidic patch (residues 59−61), and the exposed heme edge is near the hydrophobic patch. (D) Maximum-overlap configuration (MAX OV): the heme edge points to the acidic patch, so that Cys 17 is near Tyr 83. (E) Southern equatorial configuration (S/EQ): the heme edge points between the lower part of the acidic patch and the "southern" (bottom) end of cupriplastocyanin. (F) Minimum-distance configuration (MIN DIST): the heme edge points at the His 87 in the hydrophobic patch, and the iron(II)−copper(II) distance is minimized without regard for electrostatic factors.

toward different areas of plastocyanin. For the sake of consistency, we adopted the designations and acronyms used in the original study;[18] see the caption to Figure 2. The first five configurations shown are stabilized to similar extents by electrostatic interactions, and the minimum-distance configuration lacks electrostatic stabilization. Because the maximum-overlap configuration optimizes electrostatic interactions, it was claimed to be the configuration in which electron transfer occurs.[18] This claim contradicts considerable experimental evidence that the docking orientation and the reactive orientation need not be identical and that electron transfer is modulated by rearrangement of the electrostatic complex.[20−26] Although the computational procedure of Roberts et al. is impressive for the efficiency with which it identifies favorable protein−protein *interactions*, electron-transfer *reactions* seem to require more than complementarity of electrostatic fields.[65] In this study, we investigate the importance of electronic coupling between the donor and the acceptor for the electron-transfer reactions.

Results and Discussion

First Comparison of the Cyt/Pc Configurations. Effects of Tunneling Distance. If proteins are viewed as structureless, isotropic barriers to electron tunneling, the rate of this process is expected to depend exponentially on donor−acceptor distance.[49] We assumed the reorganization energy of 1.0 eV[1−8] and calculated[49b] the relative rate constants for the reaction in eq 1 for all the six configurations of the cyt/pc complex.[18] We defined the donor−acceptor distance in four ways: the iron atom to the copper atom, the heme edge to the copper atom, the heme edge to the sulfur atom of Cys 84, and the heme edge to the δ-nitrogen atom of His 87. The order of the configurations by reactivity varied somewhat with these definitions of distance. The rate constant for the S/EQ configuration came out nearly zero under three of the definitions. The approximate overall

(65) Koppenol, W. H.; Margoliash, E. *Chemtracts: Biochem. Mol. Biol.* **1992**, *3*, 110.

Table 1. Best Electron-Tunneling Paths from Fe(II) to Cu(II) in Six Configurations of the Cyt/Pc Complex Shown in Figure 2, Calculated for Three Levels of Hydration and with Two Parametrizations of Coupling within the Aromatic Rings (ϵ Values)

	10^{10} (relative coupling)^2 for the best path					
	no H_2O		internal H_2O		internal and external H_2O	
cyt/pc config	$\epsilon = 0.6$	$\epsilon = 1$	$\epsilon = 0.6$	$\epsilon = 1$	$\epsilon = 0.6$	$\epsilon = 1$
N/EQ	100	290	100	290	100	290
MAX OV ROT	0.31	6.7	5.6	120	5.6	120
MAX CHAR	11	87	11	87	11	87
MAX OV	0.15	3.1	0.59	13	0.97	13
S/EQ	7.2×10^{-5}	9.5×10^{-5}	4.9×10^{-5}	1.1×10^{-2}	4.9×10^{-5}	1.1×10^{-2}
MIN DIST	1.2×10^{3}	9.5×10^{3}	4.3×10^{3}	3.4×10^{4}	4.3×10^{3}	3.4×10^{4}

order, from the most reactive to the least reactive configuration, was as follows: MIN DIST, MAX CHAR, N/EQ, MAX OV, MAX OV ROT, and S/EQ.

In the *Pathways* method, the proteins are viewed as structured barriers providing discrete paths for electron tunneling. Different analyses by this method gave somewhat different but fairly consistent results, as explained below, but the overall findings from these analyses differ from the aforementioned overall finding by the simple exponential model. The rest of this article is devoted to the analyses in terms of tunneling paths.

Second Comparison of the Cyt/Pc Configurations. Effects of Water and of Aromatic Groups. We searched the paths in all the configurations of the cyt/pc complex shown in Figure 2. We examined the effect of water on electron tunneling by considering each configuration without water, with water inside the proteins, and with water both inside the proteins and near the interface. We compared two parametizations for the aromatic systems—as usual covalent bonds with attenuated coupling and as fully delocalized systems with unattenuated coupling. The results are in Table 1. The rate constant for electron transfer is proportional to the square of the electronic coupling, as in eq 11.

Myriad paths were found because those differing in a single orbital are considered different. Because many paths are interdependent, the matrix element T_{DA} is not simply a sum over all the paths linking the iron and copper atoms[39] but each additional path slightly affects the overall electronic coupling. As expected, the minimum-distance configuration provides by far the best coupling because it was constructed to provide it. Of the five realistic, electrostatically-stabilized configurations, the northern equatorial one seems to have the most efficient best path. In most cases, neglect of the attenuation in aromatic systems enhances the coupling without changing the route of the best path. The southern equatorial configuration is the only one in which the best (in a relative sense) path changes when the parametrization of the aromatic systems is changed, but all the paths in this configuration are very inefficient, and the apparent change in the least inefficient one may be a calculational artifact of little significance. Making the aromatic systems unattenuated benefits six-membered rings such as that in Tyr 83 (involved in the maximum-overlap and southern equatorial configurations) more than five-membered rings such as that in His 87 (involved in the northern equatorial, maximum-charge, and minimum-distance configurations). Two tunneling steps occur entirely within a six-membered ring, whereas only one step occurs entirely within a five-membered ring. The largest aromatic system, heme, when parametrized to be unattenuated allows many possibilities for an electron to "roam around" while still tunneling "forward". Since, however, heme is involved in all the paths, this factor probably does not change the qualitative results of the analysis.

Internal hydration improves coupling in the maximum-overlap configuration and in the related configuration derived by rotation of cytochrome *c* by 180° (designated maximum overlap, rotated) because these configurations involve Tyr 83, near which sits a water molecule. External hydration seems to affect coupling only marginally. The slight increase, from 0.59 to 0.97, in the case of the maximum-overlap configuration seems to be a harmless artifact, resulting in a reversal of the ranking of the best and next-best paths. In view of the approximations involved in these searches and calculations, such small changes should not be overinterpreted.

Two qualitative findings are especially interesting. The best path in the maximum-overlap configuration does not seem to involve Cys 17. The northern equatorial configuration seems to provide the best single path even though this path does not involve aromatic groups and water molecules and, therefore, does not benefit from the unattenuated aromatic coupling and hydration.

Some routine applications of the *Pathways* method amount to identification and comparison of the good or the best tunneling paths in a given protein or a series of protein derivatives. But even the less efficient paths need to be considered because they, too, contribute to the total coupling between sites. Study of interaction (interference) among multiple paths is beginning,[39] but it is not yet clear how this intricate problem can be solved correctly. In the absence of an accepted method, we intuitively addressed the qualitative question: Are many good paths more or less efficient than few excellent ones? We analyzed the results of the calculations given in the last column in Table 1 and for each configuration found the number of paths with relative couplings in the decile intervals 100−90%, 90−80%, ..., down to 40−30% relative to that in the best path. These distributions were generally similar for all the configurations of the cyt/pc complex. Because the interference among the paths can be both constructive and destructive,[66-68] and because of the ways in which rings of different sizes (e.g., phenyl vs imidazole) are treated in the *Pathways* method, neither the number of paths nor the relative coupling that they provide is evidence for or against the importance of multiple paths. In our intuitive analysis, however, it seems unlikely that the lack of excellent paths (as in the maximum-overlap configuration) is compensated by an abundance of good ones. Although this nonrigorous finding may lend some credence to the practice of considering only the most efficient path or paths, our intuition may be wrong. The growing practice of considering only the best tunneling paths should be analyzed theoretically.

Third Comparison of the Cyt/Pc Configurations. Search for New Paths. Because of the approximations in the *Pathways* method, even the relative magnitudes of the coupling in Table 1 must be taken skeptically. Paths more efficient than those in Table 1 may conceivably be discovered by more rigorous calculations. We sought additional paths by widening the search to include relative couplings down to less than 1% of that in the best path for a given cyt/pc configuration. The extended search takes a long time and requires much memory. To make it possible, we systematically "removed" from the best paths

Table 2. Analysis of the Best Electron-Tunneling Path, Listed in the Last Column of Table 1, in Each of the Six Configurations of the Cyt/Pc Complex Shown in Figure 2[a]

cyt/pc config	path no.	blocked[b]	variable segment of the path[c] Fe−heme···−Cu	10^{10} (rel coupl)^2	10^{10} (rel coupl)^2 if $\epsilon = 1$ for Cu(II)−Cys 84	γ_{AL} 10^{10}(rel coupl)^2	γ_{AL}^2 10^{10}(rel coupl)^2
N/EQ	1	none	-Cys 17/Gly 89-Gln 88-His 87	287	287	32	3.4
	2	Gly 89	/Gln 88-His 87	29	29	3.2	0.35
	3	Gln 88	/pc Gly 89/cyt Gln 16/pc H_2O/His 87	28	28	3.1	0.33
	4	His 87 sc	-Cys 14-Lys 13/pc H_2O/Ser 85-Cys 84	13	37	8.8	6.2
	5	His 87 sc, Cys 84 sc	/Gly 89/Ala 90-Gly 91-Met 92	13	13	0	0
MAX OV ROT	1	none	-Cys 17/pc H_2O/Tyr 83-Cys 84	121	336	82	56
	2	Cys 84	-Cys 17/pc H_2O/Tyr 83-Met 92	0.54	0.54	0	0
	3	Tyr 83 sc	-Cys 17/pc H_2O/Phe 41-Val 40/Tyr 83-Cys 84	0.47	1.3	0.32	0.22
	4	Tyr 83	-Cys 17/pc H_2O/Phe 41-Val 40-Ile 39-Asn 38-His 37	2.2×10^{-2}	2.2×10^{-2}	2.4×10^{-3}	2.7×10^{-4}
MAX CHAR	1	none	-Cys 17-Gln 16/His 87	87	87	9.6	1.0
	2	Gln 16	/cyt H_2O/His 87	6.1	6.1	0.67	7.4×10^{-2}
	3	His 87 sc	-Cys 14-Lys 13-Gln 12/Ser 85-Cys 84	0.63	1.7	0.43	7.5×10^{-3}
	4	His 87 sc, Ser 85	-Cys 14-Lys 13-Gln 12/Cys 84	0.38	1.0	0.26	4.5×10^{-3}
	5	His 87 sc, Lys 13	-Cys 17/Pro 86-Cys 84	0.31	0.85	0.21	0.14
MAX OV	1	none	/Tyr 83-Cys 84	13	35	8.8	5.8
	2	Tyr 83 sc	/sol H_2O/pc H_2O/Ser 85-Cys 84	0.80	2.2	0.54	0.37
	3	Tyr 83 sc, Cys 84 sc	/sol H_2O/pc H_2O/Ser 85-Pro 86-His 87	0.11	0.11	1.2×10^{-2}	1.3×10^{-4}
	4	Tyr 83 sc, Ser 85	/pc H_2O/Gln 88-His 87	4.3×10^{-2}	4.3×10^{-2}	4.7×10^{-3}	5.1×10^{-4}
	5	Tyr 83 sc, Cys 84 sc, Ser 85, His 87 sc	-Cys 17/Glu 59/Asn 38-His 37	1.4×10^{-3}	1.4×10^{-3}	1.5×10^{-4}	1.7×10^{-5}
S/EQ	1	none	-Cys 14-Lys 13/pc H_2O/Tyr 83-Cys 84	1.1×10^{-2}	2.9×10^{-2}	7.5×10^{-3}	4.9×10^{-3}
	2	Tyr 83 sc	/cyt H_2O/Glu 43-Asp 42-Phe 41-Val 40/Tyr 83-Cys 84	2.3×10^{-4}	6.1×10^{-4}	1.6×10^{-4}	1.0×10^{-4}
MIN DIST	1	none	-Cys 17/pc H_2O/Val 28/His 87	3.4×10^{4}	3.4×10^{4}	3.7×10^{3}	410
	2	His 87	/Pro 36-His 37	6.1×10^{3}	6.1×10^{3}	670	73
	3	Val 28	-His 87	360	360	40	4.3

[a] Effects on relative coupling of the following adjustments: blocking of amino acids or of their side chains (sc); neglect of coupling attenuation ($\epsilon = 1$) in the bond between Cu(II) and the thiolate S atom of Cys 84; the scaling of Cu(II)−ligand coupling by the expansion coefficient (γ_{AL}) or by the square of the expansion coefficient (γ_{AL}^2) describing the ligand contribution to the redox molecular orbital of the blue copper(II) site. [b] sc, only the side chain. [c] Dash represents a bond, slash represents a contact through space. All paths end with a ligand bonded to Cu(II). Water "belongs" to either protein or to the solvent.

certain amino acid residues or just their side chains by neglecting the coupling interactions involved. The results are given in the first five columns in Table 2. Most of the newly-found paths overlap with (i.e., involve some orbitals along) the best path in each configuration. In the minimum-distance configuration, which lacks electrostatic stabilization and is therefore unlikely to participate in the electron-transfer reaction, the new path 2 does not overlap with the best path and provides as much as 20% of the relative coupling of the latter. In the five electrostatically-stabilized configurations there are four new paths that do not overlap the best paths, but they have relative couplings less than 10% of that in the corresponding best path. Paths 2 and 3 in the maximum-overlap configuration involve water of solvation and probably would not have been found if external solvation were neglected. The most interesting among the new paths are paths 4 and 5 in the northern equatorial configuration. They do not overlap with each other, nor with the best path in this configuration, and are as efficient as the best path in the maximum-overlap configuration. Although the numerical couplings in Table 2 may be inaccurate in the absolute sense, we believe that the 24 paths listed are a realistic set. Better calculations undoubtedly would give different numbers and probably would yield different rankings of some of these paths but probably would not turn up additional efficient paths not contained in Table 2.

Again, at this stage of analysis, the northern equatorial configuration appears best suited for electron transfer, and the maximum-overlap configuration appears noncompetitive without a rearrangement. Rotation of the cytochrome *c* molecule by 180°, which yields the "maximum-overlap, rotated" configuration, seems to improve the iron−copper coupling beyond that achieved in the non-rearranged maximum-overlap configuration.

Fourth Comparison of the Cyt/Pc Configurations. Allowances for Anisotropy of Copper−Ligand Coupling. Because all electron-tunneling paths begin at the porphyrin nitrogen atoms, different coupling of the iron(II) to its axial (His 18 and Met 80) and equatorial (porphyrin) ligands is unimportant for this analysis. Because, however, different paths end at different ligands to the copper(II) atom, anisotropy of coupling within the blue copper site is important for electron transfer. We recognize the high covalency and the π character of the copper(II)−thiolate bond in three ways, all of which favor the paths ending with Cys 84 and disfavor those ending with the other three ligands—imidazole rings of His 37 and His 87 and the thioether group of Met 92.

When the attenuation of coupling in the Cu(II)−Cys 84 bond is neglected by setting $\epsilon = 1$ for this bond, the best path in the "maximum-overlap, rotated" configuration matches or exceeds the best path in the northern equatorial configuration. Even with the enhancement of its best path, the maximum-overlap configuration lags behind these other two configurations.

Scaling of the relative couplings by the expansion coefficients, or by the squares of the coefficients, of the ligand orbitals in the blue copper HOMO sligthly changes the relative ranking of paths and configurations. Path 4 in the northern equatorial configuration, which ends with Cys 84, approaches or exceeds path 1, which ends with His 87. The rankings within other configurations remain unchanged. The main "beneficiary" of the adjustment for anisotropy of coupling is the "maximum-overlap, rotated" configuration. Its best path, which ends with Cys 84, emerges as the best one of all. Path 2 in this configuration, which ends with Met 92, is abolished because this ligand does not significantly contribute to the redox molecular orbital. Indeed, the bond of Met 92 to copper(II) is

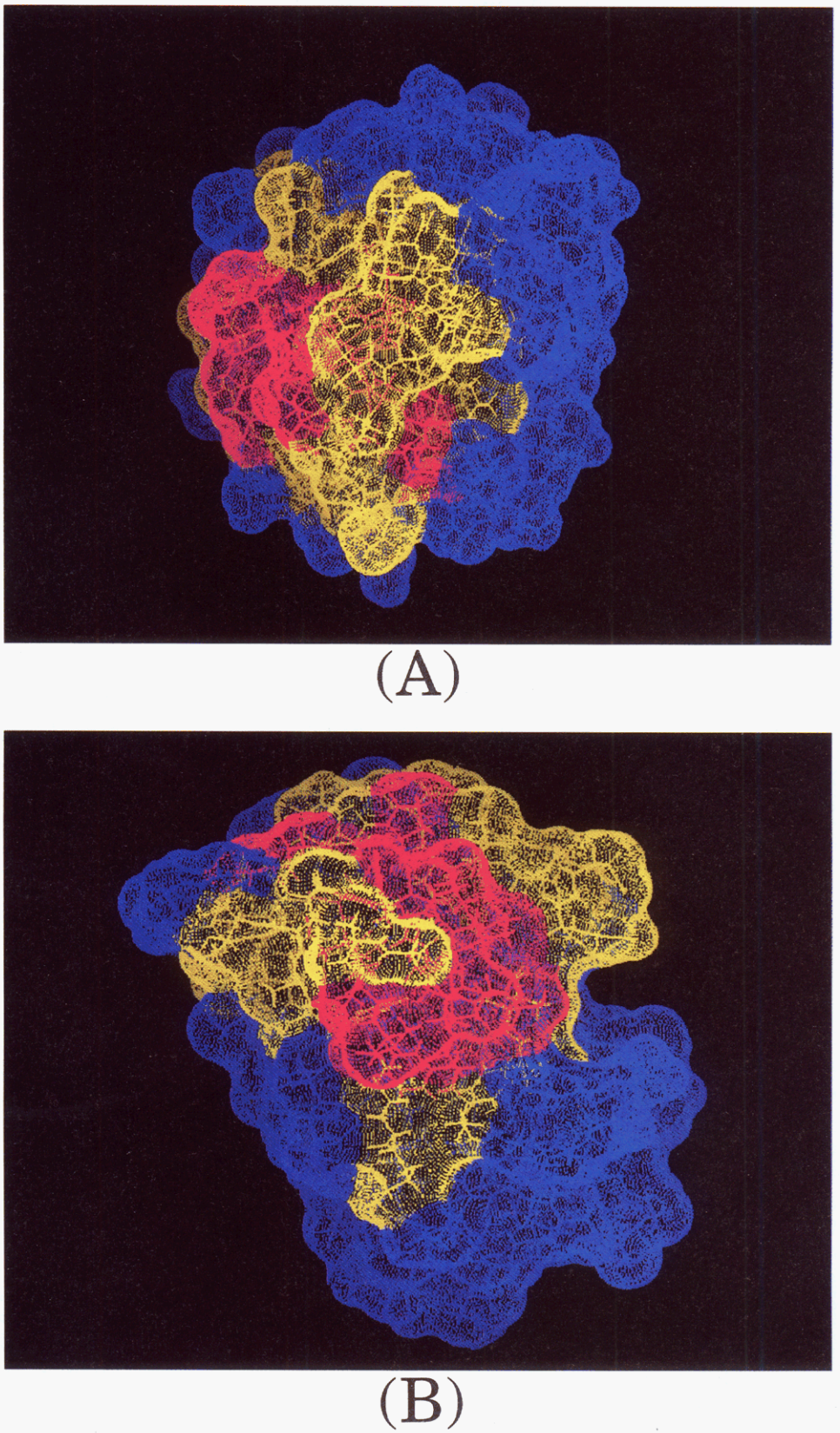

Figure 3. Electronic coupling of the protein surface to the metal atom in (A) tuna ferrocytochrome *c* and (B) poplar cupriplastocyanin. Both protein molecules are shown as in the "maximum-overlap, rotated" configuration, except that each molecule is swung by 45° so that the interfacial areas partially face the viewer. Strong coupling is marked in red, medium coupling in yellow, and weak coupling in blue.

longer and weaker than the bonds of the other three ligands.[13b,56–58]

At this stage of the analysis, the maximum-overlap configuration still remains noncompetitive for electron transfer. Its best path, via a heme methyl group, is comparable only to the best in the northern equatorial configuration and lags behind the best in the "maximum-overlap, rotated" configuration, via Cys 17. The maximum-charge configuration is comparable to the maximum-overlap configuration. The southern equatorial

(66) Liang, C.; Newton, M. D. *J. Phys. Chem.* **1992**, *96*, 2855.
(67) Siddarth, P.; Marcus, R. A. *J. Phys. Chem.* **1993**, *97*, 6111.
(68) Gruschus, J. M.; Kuki, A. *J. Phys. Chem.* **1993**, *97*, 5581.

configuration remains insignificant. The minimum-distance configuration, which lacks electrostatic stabilization, is included for the sake of completeness.

Coupling Maps of the Separate Proteins. So far we discussed electronic coupling between the redox sites inside the two protein molecules by analyzing tunneling paths through the diprotein complex, cyt/pc, in its different configurations. Now we analyze the coupling between the redox site and the protein surface for both proteins separately, and then we consider interactions of the two protein molecules via their surfaces. Comparative analyses showed only slight differences in the coupling maps of the same protein in the oxidized and reduced forms and between different species of the same protein—cytochrome *c* from tuna and horse and plastocyanin from poplar and bean. We briefly discuss tuna ferrocytochrome *c* and polar cupriplastocyanin. Similar analyses of coupling in these proteins were made for purposes different from ours.[36,38]

The following residues on the cytochrome *c* surface are relatively strongly coupled to the iron(II) atom, and they define the larger red area in Figure 3A: Cys 14, Cys 17, Val 28, Pro 30, Asn 31, Lys 79, Met 80, and Ile 81. A small part of the backbone (but not the imidazole ring) of His 18 and the residue Thr 19 define the smaller red area. The partially exposed heme edge is in that part of the larger red area that borders the prominent yellow area in Figure 3A. The yellow bulge in the bottom center of Figure 3A is Lys 27.

The following residues on the plastocyanin surface are relatively strongly coupled to the copper(II) atom: Ala 33, Gly 34, Pro 36, Phe 82, Tyr 83, Ser 85, Pro 86, His 87, Gln 88, Gly 91, and Val 93. The hydrophobic patch is the red area in the top center of Figure 3B. The acidic residues 59−61, which constitute the cluster in the acidic patch that is close to the hydrophobic patch, are the medium-coupled yellow area on the upper right side. The acidic residues 42−44, which constitute the cluster in the acidic patch that is remote from the hydrophobic patch, are the weakly-coupled blue area in the center right of Figure 3B. The strongly-coupled red area between the two acidic clusters includes Tyr 83 and is contiguous with the hydrophobic patch. The blue bulge on the right side contains Asp 51.

Surface Interactions in Two Configurations of the Cyt/Pc Complex. The relatively weak electronic coupling between the iron(II) and copper(II) sites in the maximum-overlap configuration may be caused by the relatively large gap between the surfaces of the two proteins. The protein surfaces facing each other in this configuration are well coupled to their respective metal atoms, but the contact between those surfaces is weak. Although Ile 81 is relatively strongly coupled to the iron(II) atom, protrusion of this residue and of Ala 83 shields from plastocyanin the most strongly coupled group in cytochrome *c*—the porphyrin. Although Tyr 83 is strongly coupled to the copper(II) atom, this aromatic residue sits between the two protruding clusters of acidic residues. Because of these steric factors, the distance between the solvent-exposed heme edge and Tyr 83 is too large for efficient electron tunneling.

The northern equatorial configuration, which emerged as one of the two configurations most favorable for electron transfer, does not suffer from steric problems. The heme edge sits between His 87 and Tyr 83, two residues in plastocyanin that are strongly coupled to the copper(II) atom. Moreover, the residue Cys 17 in cytochrome *c*, which is strongly coupled to the iron(II) atom, interacts well with the hydrophobic patch in plastocyanin. These two simultaneous interactions make the northern equatorial configuration especially favorable for electron transfer.

Conclusions

The so-called northern equatorial and "maximum-overlap, rotated" configurations of the electrostatic complex cyt/pc seem to provide the strongest electronic coupling between the iron(II) and copper(II) sites and the most efficient tunneling paths. The maximum-overlap configuration, in which electrostatic interactions are optimized, remains noncompetitive with these two configurations regardless of the parametrization used in the *Pathways* calculations and regardless of the method by which these calculations are corrected for anisotropy of coupling in the blue copper site. These consistent theoretical findings corroborate and explain the experimental findings in this laboratory, that the configuration optimal for protein docking is not optimal for subsequent electron-transfer reaction between the docked proteins and that a rearrangement is involved.[20−26] A rearrangement of the maximum-overlap configuration to its "rotated" version is a nice example of configurational fluctuation, in which the basic patch in cytochrome *c* and the acidic patch in plastocyanin remain close to each other while the protein−protein orientation changes. A rearrangement of the maximum-overlap configuration to the northern equatorial configuration has the characteristics of both configurational fluctuation and migration; in the latter rearrangement, the basic patch surrounding the exposed heme edge in cytochrome *c* moves from the acidic patch toward or into the hydrophobic patch on the plastocyanin surface. These theoretical findings support another view, which emerged from very recent experimental studies in our laboratory—that configurational fluctuation and migration of the proteins on each other's surfaces are dynamical processes that should not be sharply distinguished because they differ in degree more than in kind.[32] Cytochrome *c* and plastocyanin are prototypical metalloproteins, and the dynamic phenomena examined here are likely to be found in other protein systems as well.

The *Pathways* method for analysis of electron-tunneling paths can be profitably applied to metalloprotein complexes, in which both the donor and the acceptor are embedded in the protein matter. Internal and external hydration, anisotropy of metal−ligand coupling, and steric effects should all be considered, and this method will surely be improved in other ways. Trends in calculated couplings, not their numerical values, should be analyzed. Then the *Pathways* method may give insight into electron tunneling through proteins and may guide experimentalists in the design of studies involving protein mutants.

Acknowledgment. This work was supported by the NSF (Grant MCB-9222741) and the A. P. Sloan Fellowship to N.M.K. and by a travel grant by the German National Scholarship Foundation to G.M.U. We thank Drs. Elizabeth D. Getzoff and Victoria A. Roberts for atomic coordinates of the cyt/pc complex in six configurations, Jeffrey J. Regan for instructions for use of the program Greenpath v0.90, and Dr. M. Mercedes Silva for help with computer graphics.

JA941958V